# Exact Green's functions for a Brownian particle reversibly binding to a fixed target in a finite, two-dimensional, circular domain

**Ziya Kalay**

Institute for Integrated Cell-Material Sciences (WPI-iCeMS), Kyoto University, Kyoto, 606-8501, Japan

E-mail: zkalay@icems.kyoto-u.ac.jp

**Abstract.** Despite the apparent need to study reversible reactions between molecules confined to a two-dimensional space such as the cell membrane, exact Green's functions for this case has not been reported. Here we present exact analytical Green's functions for a Brownian particle reversibly reacting with a fixed reaction center in a finite two-dimensional circular region with reflecting or absorbing boundaries, considering either a spherically symmetric initial distribution, or a particle that is initially bound. We show that the Green's function can be used to predict the effect of measurement uncertainties on the outcome of single particle/molecule tracking experiments in which molecular interactions are investigated. Hence, we bridge the gap between previously known solutions in one-dimension (Agmon N 1984 J. Chem. Phys. 81:2811) and three-dimensions (Kim H and Shin K J 1999 Phys. Rev. Lett. 82:1578), and provide an example of how the knowledge of the Green's function can be used to predict experimentally accessible quantities.

PACS numbers: 05.40.-a, 82.20.Fd, 83.10.Mj

Submitted to: *J. Phys.* A

## 1. Introduction

A theoretical study of the kinetics of colloid coagulation by Smoluchowski [1] stimulated much of the theoretical research done in the study of bimolecular reactions. Smoluchowski's formulation, in the context of bimolecular reactions, involves solving the diffusion equation in the presence of an infinite amount of available reactants which react immediately at an interaction distance. These reactions are called *diffusion limited reactions* as the rate of the reaction is controlled by the rate at which the particles encounter. In general, the particles do not necessarily react during their first encounter. In order to take this effect into account, Collins and Kimball suggested the use of a different boundary condition, the so-called radiation boundary condition, which allows for neutral encounters [2]. The radiation boundary condition was considered by Naqvi and collaborators, who also gave an exact solution for the time-dependent reaction rate in two-dimensions [3]. Later, Agmon and Szabo [4] gave a generalization of Smoluchowski's approach for the case of reversible reactions. Another approach to this problem was developed by Noyes [5]. In Noyes' theory, one considers a counterpart of the system of interest, identical to the original system except that the reactants are not consumed upon encounter. The central quantity in this theory is the probability of first reencounter between a reference reactant and the rest of the reactants at time $t$, given there was an encounter at $t = 0$. The reaction rate in the original system was shown to be related to the reencounter time distribution in the nonreactive system, and its asymptotic value was obtained [5]. More recently, Noyes' approach has been revived, and a calculation of the reencounter time distribution based on molecular dynamics simulations was given [6]. It is also worthwhile to note that in this approach, the transport of reactants does not need to be diffusive. Later on, Torney and McConnell showed that Noyes and Smoluchowski theories are equivalent on a lattice [7]. Lastly, we would like to note the recent work of Fange et al. [8] that establishes relations between different spatially and temporally resolved models for reaction kinetics at different levels of detail.

In this article, we present exact analytical solutions for a Brownian particle reversibly binding to a fixed target in a finite two-dimensional circular domain, by calculating the Green's function of the Smoluchowski equation with appropriate boundary conditions. We restrict our analysis to spherically symmetric initial distributions, and the case where the particle and the target are initially bound. Previously, Green's functions for a pair of isolated particles undergoing reversible reaction were given in one-dimension (1D) [9] and in three-dimensions (3D) [10], but a solution for two-dimensions (2D) has been missing, despite the obvious importance of chemical kinetics in 2D surfaces such as the cell membrane. We believe that our results further expand the applicability of the already developed methods in the literature to 2D systems. For instance, the knowledge of the Green's function enables one to calculate the survival probability, which is closely related to the time-dependent reaction rate (see for instance Agmon and Szabo [4]). Moreover, we contribute to theory of

reaction kinetics in a finite domain. It is well-known that the reaction rate in an infinite 2D domain asymptotically vanishes due to insufficient influx of reactants due to low dimensionality [11]. However, it is possible to define an asymptotic reaction rate for a finite 2D domain, and our results can be applied to cases where spherical symmetry exists. In addition, the probability distributions we obtain here can be used to calculate quantities related to reencounter time statistics in finite 2D systems that possess spherical symmetry, within the Noyes formalism [5, 6]. To give an example of how our findings can be applied to practical problems, here we also provide a calculation regarding the effect of measurement procedures on the outcome of single particle/molecule tracking experiments conducted to investigate molecular interactions in surfaces such as the plasma membrane of live cells. Moreover, our analytical results can be used to simulate a 2D system of many particles that diffuse and reversibly react, via the *Green's function reaction dynamics* method [12, 13].

## 2. Green's functions in a finite 2D disc with reflecting or absorbing boundaries

### *2.1. For a particle and reaction center that are initially separated*

Consider a Brownian particle in a circular region of radius $b$ that interacts with a circular target at $r = a$ (see figure 1 (a) for an illustration of the problem). The probability density of finding the particle at position $\vec{r}$ obeys the Smoluchowski equation [4]

$$\frac{\partial \rho(\vec{r},t)}{\partial t} = \nabla \cdot D(\vec{r}) \left( \nabla + \frac{1}{k_{\mathrm{B}}T} \nabla U(\vec{r}) \right) \rho(\vec{r},t), \tag{1}$$

where $D(\vec{r})$ is the relative diffusion coefficient, $k_{\mathrm{B}}$ is the Boltzmann constant, $T$ is the temperature, and $U(\vec{r})$ represents the interaction potential. Here, we consider the case in which particles only interact on contact, so that the interaction potential in equation (1) is put to zero, and a reaction boundary condition is implemented. In 2D, and when the initial distribution of the Brownian particle is spherically symmetric, equation (1) reduces to

$$\frac{\partial \rho}{\partial t} = D \frac{1}{r} \frac{\partial \rho}{\partial r} \left( r \frac{\partial \rho}{\partial r} \right), \tag{2}$$

where the diffusion coefficient is taken to be constant. When the separation between the Brownian particle and the target is equal to $a$, the particle can reversibly bind to the target. To account for this, we employ the so called *back reaction* boundary condition at $r = a$, which is given by [9, 10]

$$2\pi a D \left. \frac{\partial \rho(r,s)}{\partial r} \right|_{r=a} = 2\pi a D k_{\mathrm{r}} \rho(a,s) - D k_{\mathrm{d}} \left[ 1 - S(s) \right], \tag{3}$$

where $k'_{\mathrm{r}} = 2\pi a D k_{\mathrm{r}}$ and $k'_{\mathrm{d}} = D k_{\mathrm{d}}$ are the rates of forward (association) and backward (dissociation) reactions, respectively, $S(s)$ is the probability that the reactants are not forming a dimer at $s$, i.e. the *survival probability*, given by

$$S(s) = 1 - 2\pi a \int_0^s du \left. \frac{\partial \rho(r,u)}{\partial r} \right|_{r=a}, \tag{4}$$

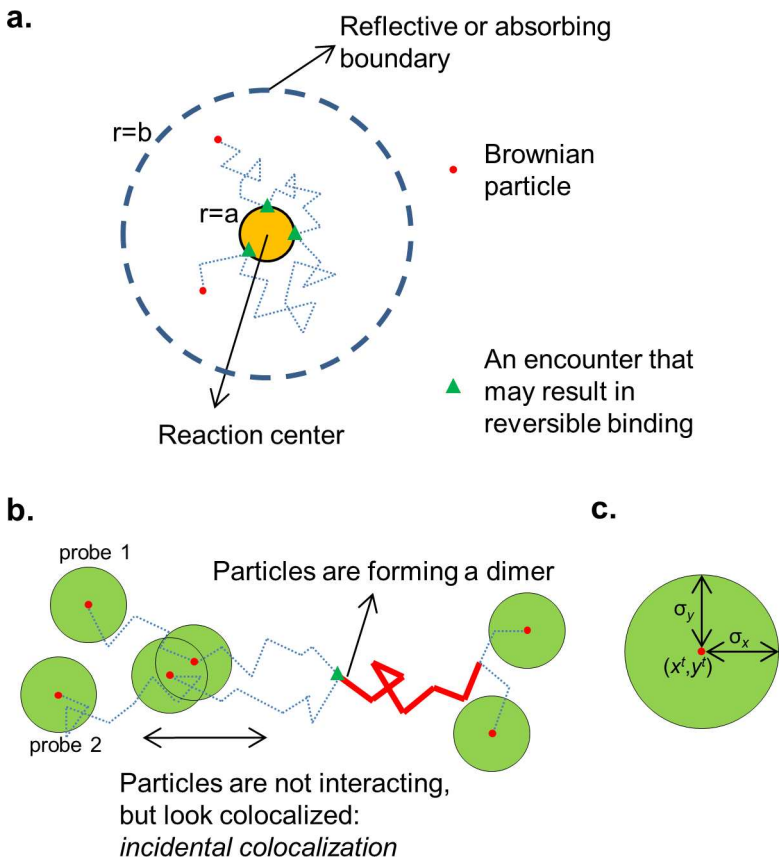


**Figure 1.** **a.** Schematic illustration of a Brownian particle (red dot) reversibly binding to a reaction center (orange disc), or target, at $r = a$, in a circular region of radius $b$ whose boundary is either reflective or absorbing. Dotted lines represent the random trajectory of the particle. When the particle encounters the target, it may bind reversibly, such that the association rate is $k'_{\mathrm{r}}$ and the dissociation rate is $k'_{\mathrm{d}}$, as described in the text. **b.** Illustration of the effect of uncertainty in position measurements. The trajectories of two Brownian particles, or probes, that can reversibly dimerize are shown. The red dots correspond to the particles, but their measured positions could lie in a greater area shown by the larger (green) circles due to measurement errors, as shown in detail in **c** (see section 3 for a detailed explanation). When the particles are forming a dimer, their common trajectory is indicated by thick red line segments. In single particle/molecule tracking experiments, the position of a probe can be determined up to a certain precision, which can be much larger than the radius of the molecule. Therefore, even if two molecules are not interacting, they will look colocalized when the distance between them is comparable or smaller than the position precision, such that it is not possible to say whether the molecules are bound or not. These events can be referred as *incidental colocalizations*.

and we defined the time-like variable $s = Dt$ for brevity in notation. In many physically relevant situations, the particle and the target are in a finite space with reflecting or absorbing boundaries, such that we consider one of the following boundary conditions at $r = b$

$$\left.\frac{\partial \rho(r,s)}{\partial r}\right|_{r=b} = 0, \tag{5}$$

$$\rho(b,s) \qquad = 0, \tag{6}$$

where equations (5) and (6) correspond to reflective and absorbing boundaries at $r = b > a$, respectively.

It is extremely useful to note that the solution of equation (2) can be expressed as $\rho(r,s) = G(r,s|r_0,0) + f(r,s)$, where $G(r,s|r_0,0)$ is the Green's function for equation (2) with reflective boundary condition at $r = a$, and $f(r,s)$ is a function that vanishes everywhere at $s = 0$ and satisfies the back reaction boundary condition, equation (3), at $r = a$ and that both functions satisfy reflecting or absorbing boundary conditions at $r = b$. Let $\rho^{(1)}(r,s) = G^{(1)}(r,s|r_0,0) + f^{(1)}(r,s)$ and $\rho^{(2)}(r,s) = G^{(2)}(r,s|r_0,0) + f^{(2)}(r,s)$ be the solutions of equation (2) that satisfy the reflective and absorbing boundary conditions at $r = b$, respectively, and the back reaction boundary condition at $r = a$, with the initial condition $\rho(r,0) = \delta(r - r_0)/2\pi r_0$. The functions $G^{(1)}(r,s|r_0,0)$ and $G^{(2)}(r,s|r_0,0)$ are well-known, and are given by [14]

$$\begin{aligned} G^{(1)}(r,s|r_0,0) &= \sum_{n=1}^{\infty} g_n^{(1)}(r|r_0) e^{-\alpha_n^2 s} + \frac{1}{\pi(b^2-a^2)} \\ &= \frac{\pi}{4} \sum_{n=1}^{\infty} \frac{J_1^2(b\alpha_n)}{F^{(1)}(\alpha_n)} C_0^{(1)}(r,\alpha_n) C_0^{(1)}(r_0,\alpha_n) e^{-\alpha_n^2 s} + \frac{1}{\pi(b^2-a^2)}, \end{aligned} \tag{7}$$

$$G^{(2)}(r,s|r_0,0) = \sum_{n=1}^{\infty} g_n^{(2)}(r|r_0) e^{-\beta_n^2 s} = \frac{\pi}{4} \sum_{n=1}^{\infty} \frac{J_0^2(b\beta_n)}{F^{(2)}(\beta_n)} C_0^{(2)}(r,\beta_n) C_0^{(2)}(r_0,\beta_n) e^{-\beta_n^2 s}, \tag{8}$$

where

$$\begin{aligned} F^{(1)}(\alpha_n) &= J_1^2(a\alpha_n) - J_1^2(b\alpha_n), \\ C_0^{(1)}(r,\alpha_n) &= \alpha_n [J_0(r\alpha_n) Y_1(a\alpha_n) - Y_0(r\alpha_n) J_1(a\alpha_n)], \\ F^{(2)}(\beta_n) &= J_1^2(a\beta_n) - J_0^2(b\beta_n), \\ C_0^{(2)}(r,\beta_n) &= \beta_n [J_0(r\beta_n) Y_1(a\beta_n) - Y_0(r\beta_n) J_1(a\beta_n)], \end{aligned}$$

$J_n(x)$ and $Y_n(x)$ are Bessel functions of the first and second kind, $\alpha_n$'s and $\beta_n$'s are the positive solutions of $J_1(a\alpha)Y_1(b\alpha) - Y_1(a\alpha)J_1(b\alpha) = 0$ and $-J_1(a\beta)Y_0(b\beta) + Y_1(a\beta)J_0(b\beta) = 0$, respectively, and $g_n^{(i)}(r|r_0)$'s are implicitly defined in the equalities.

In this study, we calculate $f^{(1)}(r,s)$ and $f^{(2)}(r,s)$ by the Laplace transform method. The Laplace transform of equation (2) yields the well-known modified Bessel differential equation [14] with the solution $\widetilde{\rho}(r,\epsilon) = AI_0(r\sqrt{\epsilon}) + BK_0(r\sqrt{\epsilon})$, where $I_n(x)$ and $K_n(x)$ are modified Bessel functions of the first and second kind, respectively, tilde denotes Laplace transform, and $\epsilon$ is the Laplace transform variable. The arbitrary constants $A$ and $B$ are determined by imposing the boundary conditions, and the inverse Laplace transform of the resulting expressions can be exactly calculated by directly evaluating the Bromwich contour integral [14]. After long but straightforward calculations, which are given in full detail in the Appendix, we obtain

$$f^{(1)}(r,s) = k_{\mathrm{r}} \int_0^s du G^{(1)}(r,s-u|r_0,0) \sum_{n=1}^{\infty} h_n^{(1)}(r) e^{-\omega_n^2 s},$$

$$h_n^{(1)}(r) = \pi\omega_n \frac{Y_1(b\omega_n)J_0(r\omega_n) - J_1(b\omega_n)Y_0(r\omega_n)}{2C_1'(i\omega_n)}, \tag{9}$$

$$f^{(2)}(r,s) = k_{\rm r}\int_0^s du G^{(2)}(r,s-u|r_0,0)\sum_{n=1}^{\infty} h_n^{(2)}(r)e^{-\gamma_n^2 s},$$

$$h_n^{(2)}(r) = i\pi\gamma_n \frac{-Y_0(b\gamma_n)J_0(r\gamma_n) + J_0(b\gamma_n)Y_0(r\gamma_n)}{2C_2'(i\gamma_n)}, \tag{10}$$

where $\omega_n$'s are the positive solutions of

$$\begin{aligned} C_1(i\omega) = {} & \pi[(k_{\rm d}-\omega^2)/2][J_1(a\omega)Y_1(b\omega) - J_1(b\omega)Y_1(a\omega)] \\ & - (\pi k_{\rm r}\omega/2)[J_0(a\omega)Y_1(b\omega) - J_1(b\omega)Y_0(a\omega)], \end{aligned}$$

and $\gamma_n$'s are the positive solutions of

$$\begin{aligned} C_2(i\gamma) = {} & i\pi[(k_{\rm d}-\gamma^2)/2][J_0(b\gamma)Y_1(a\gamma) - J_1(a\gamma)Y_0(b\gamma)] \\ & - i(\pi k_{\rm r}\gamma/2)[J_0(b\gamma)Y_0(a\gamma) - J_0(a\gamma)Y_0(b\gamma)], \end{aligned}$$

and $C_i' = dC_i/d\epsilon$. Finally, we can express the full solutions as

$$\begin{aligned} \rho^{(1)}(r,t) = {} & G^{(1)}(r,t|r_0,0) + \frac{k_{\rm r}}{\pi(b^2-a^2)}\sum_m h_m^{(1)}(r)\frac{1-e^{-\omega_m^2 Dt}}{\omega_m^2} \\ & + k_{\rm r}\sum_{m,n} h_m^{(1)}(r)g_n^{(1)}(r|r_0)\frac{e^{-\omega_m^2 Dt} - e^{-\alpha_n^2 Dt}}{\alpha_n^2 - \omega_m^2}, \end{aligned} \tag{11}$$

$$\rho^{(2)}(r,t) = G^{(2)}(r,t|r_0,0) + k_{\rm r}\sum_{m,n} h_m^{(2)}(r)g_n^{(2)}(r|r_0)\frac{e^{-\gamma_m^2 Dt} - e^{-\beta_n^2 Dt}}{\beta_n^2 - \gamma_m^2}, \tag{12}$$

where the sums over $m$ and $n$ run over all positive integers, and the $C_i'$'s are explicitly given by

$$\begin{aligned} C_1'(i\omega) = {} & -\frac{\pi J_1(a\omega)}{4\omega}\left[b\left(k_{\rm d}-\omega^2\right)Y_0(b\omega) - \frac{2k_{\rm d} - ak_{\rm r}\omega^2}{\omega}Y_1(b\omega)\right] \\ & + \frac{\pi J_1(b\omega)}{4\omega}\left[a\left(k_{\rm d}-\omega^2\right)Y_0(a\omega) - \frac{2k_{\rm d} - ak_{\rm r}\omega^2}{\omega}Y_1(a\omega)\right] \\ & + \frac{\pi J_0(a\omega)}{4}\left[bk_{\rm r}Y_0(b\omega) - a\frac{k_{\rm d}-\omega^2}{\omega}Y_1(b\omega)\right] \\ & - \frac{\pi J_0(b\omega)}{4}\left[bk_{\rm r}Y_0(a\omega) - b\frac{k_{\rm d}-\omega^2}{\omega}Y_1(a\omega)\right], \end{aligned} \tag{13}$$

$$\begin{aligned} C_2'(i\gamma) = {} & -\frac{i\pi J_1(a\gamma)}{4\gamma^2}\left[\left(\gamma^2(-ak_{\rm r}+1)+k_{\rm d}\right)Y_0(b\gamma) + b\gamma\left(k_{\rm d}-\gamma^2\right)Y_1(b\gamma)\right] \\ & - \frac{i\pi J_1(b\gamma)}{4\gamma}\left[bk_{\rm r}\gamma Y_0(a\gamma) - b\left(k_{\rm d}-\gamma^2\right)Y_1(a\gamma)\right] \\ & - \frac{i\pi J_0(a\gamma)}{4\gamma}\left[\left(-ak_{\rm d}+a\gamma^2+k_{\rm r}\right)Y_0(b\gamma) - bk_{\rm r}\gamma Y_1(b\gamma)\right] \\ & - \frac{i\pi J_0(b\gamma)}{4\gamma^2}\left[-\gamma\left(-ak_{\rm d}+a\gamma^2+k_{\rm r}\right)Y_0(a\gamma) - \left(\gamma^2(-ak_{\rm r}+1)+k_{\rm d}\right)Y_1(a\gamma)\right]. \end{aligned} \tag{14}$$

The long-time behavior of the solutions are given by

$$\rho^{(1)}(r, s\to\infty) = \left[\pi(b^2-a^2) + 2\pi a k_{\rm r}/k_{\rm d}\right]^{-1}, \tag{15}$$

$$\rho^{(2)}(r, s \to \infty) = 0. \tag{16}$$

As expected, the steady state solution is a uniform distribution whose amplitude depends on the ratio of forward and backward reaction rates for reflective boundaries, and vanishes for absorbing boundaries.

In order to display an example of how the solution looks like, we plotted snapshots of $\rho^{(1)}(r, t)$ as a function of $r$ in figure 2, for three different values of the pair $(k_\mathrm{r}, k_\mathrm{d})$: (0, 0), (10, 2), and (10, 0.1), in arbitrary units. Note that the distributions for different cases are almost identical (see figure 2 (b)) until the particle comes appreciably close to the reactive boundary, and approaches the predicted values in the long time limit, as shown in figure 2 (f).

Before finishing this section, we would like to note that if instead we consider a pair of isolated, mobile, and spherically symmetric interacting Brownian particles, the results we gave would be applicable (when $b \gg a$) provided that the diffusion coefficient is replaced by the *relative* diffusion coefficient of the two particles. Because for a pair of isolated particles in an isotropic medium, the problem can be reformulated as that of a single particle, in which the particle diffuses around the origin with a diffusion coefficient that equals the sum of those of the original particles, and reacts whenever it is at the reaction distance from the origin [10].

### *2.2. For a particle that is initially bound to the reaction center*

Another initial configuration that could be of interest in physical applications is constituted by a particle that is bound to the reaction center. Starting from this initial state, the particle will dissociate from the reaction center at a random time $t$, which is exponentially distributed with mean $1/k'_\mathrm{d}$. Green's functions for the case of an initially separated particle-target pair can be used to express the probability distribution in the case of initially bound particles. Let $\rho(r, t|*)$ and $P(*, t|r)$ be the probability density for the distance between the particles given they were bound at $t = 0$, and the probability that the particles are bound at time $t$ given they were separated by $r$ at $t = 0$, respectively, where the asterisk stands for the bound state. As shown in Agmon and Szabo [4] and Kim and Shin [10], solutions of the Smoluchowski equation with the back reaction boundary condition satisfy a detailed balance relationship that enables us to relate $\rho(r, t|*)$ and $P(*, t|r)$ through [4, 10]

$$\begin{aligned}\rho(r, t|*) &= \frac{k_\mathrm{d}}{2\pi a k_\mathrm{r}} P(*, t|r), \\ &= \frac{k_\mathrm{d}}{2\pi a k_\mathrm{r}} \left(1 - S(t|r)\right).\end{aligned} \tag{17}$$

In the next section, we will make use of this result to calculate an observable quantity in single particle/molecule tracking experiments.

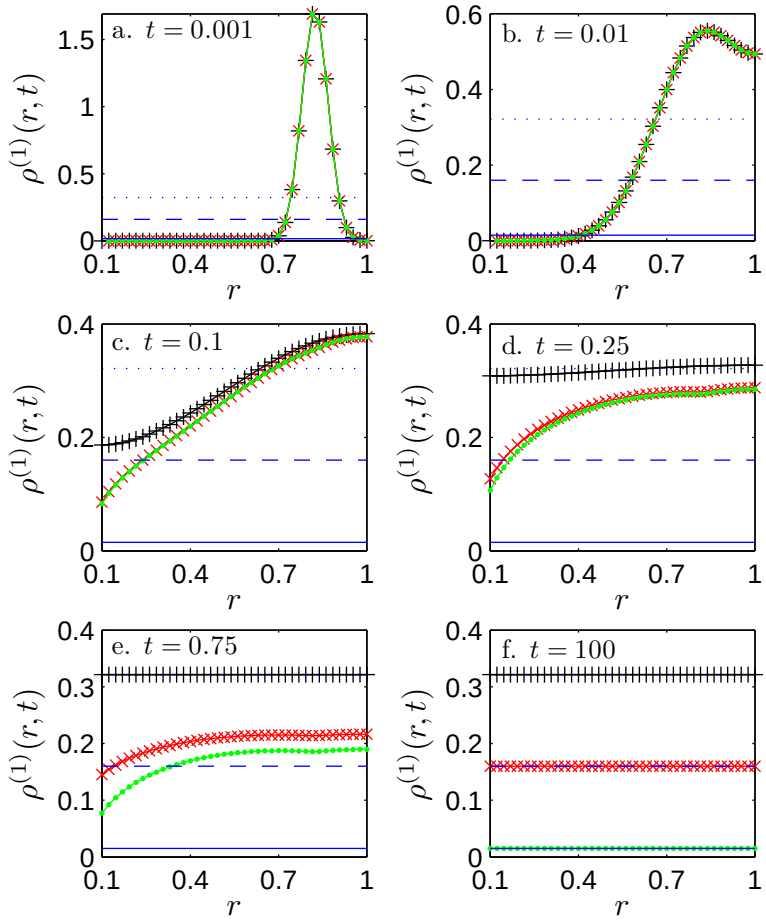


**Figure 2.** Time evolution of $\rho^{(1)}(r,t)$, which is the probability distribution in the presence of a reflecting boundary at $r = b$, given by equation (11). In each of the subfigures **a-f**, three solutions with differing $k_{\rm r}$ and $k_{\rm d}$ values are plotted as a function of $r$ at different points in time, as indicated on the figures. The dataset shown with $+$ signs (black), represent the case of no reaction; whereas the others shown with $\times$ signs (red) and dot marks (green) exemplify cases of reversible binding, with the latter being more irreversible. Parameter values are in arbitrary units, and are given by: $D = 1$, $a = 0.1$, $b = 1$, $r_0 = 3(a+b)/4$ in all curves, and the values of the pair $(k_{\rm r},\, k_{\rm d})$ are (0, 0), (10, 2), and (10, 0.1) for the data sets shown with $+$, $\times$, and dot marks, respectively, and the horizontal lines correspond to the limiting values of $\rho^{(1)}(r,t)$ as $t \to \infty$ for each case, in the same order.

## 3. Colocalization probability of interacting molecules/particles

In this section, we describe how the results obtained so far can be used to calculate the statistics of the outcome of observations made by single particle/molecule tracking techniques in the presence of measurement uncertainties. We refer to studies in the cell membrane, but our approach can be applied to any 2D system with spherical symmetry. In single particle/molecule tracking experiments whose aim is to study molecular interactions in the cell membrane, reactants are usually labelled with fluorescent probes whose emission spectra are sufficiently different [15, 16]. When the distance between

observed positions of two probes are less than a threshold value $L$, which depends on the experimental setup, the molecules can be truly interacting, such as forming a dimer, or they can just happen to be close together, which can be called *incidental colocalization* (see figure 1 (b) for an illustration).

Below, we present a calculation for the time-dependent colocalization probability for a mobile probe that behaves like a Brownian particle, and binds to a fixed probe at the center of a circular region with reflective boundaries. We take measurement errors into account by following a common scheme of modeling uncertainties in measured positions of fluorescent probes [15]. We consider two initial conditions: 1) the probes are initially not bound, and the position of the mobile probe is averaged over the circular region, 2) the probes are initially bound, and dissociate thereafter. After obtaining an equation for the colocalization probability, we display its behavior as a function of the magnitude of measurement uncertainties and the threshold $L$. We hope that our results can be used to gain insight into how measurement uncertainties would affect observed quantities without the need to perform simulations.

Let $(x_1^{\mathrm{m}}, y_1^{\mathrm{m}})$ and $(x_2^{\mathrm{m}}, y_2^{\mathrm{m}})$ be the observed positions of probe 1 and probe 2, which are the sums of *true* positions and measurement uncertainties. The components of the observed position for the $i^{\mathrm{th}}$ probe can be expressed as [15] $x_i^{\mathrm{m}} = x_i^{\mathrm{t}} + \Delta x_i + \Delta x_i^{\mathrm{o}}$ and $y_i^{\mathrm{m}} = y_i^{\mathrm{t}} + \Delta y_i + \Delta y_i^{\mathrm{o}}$, where the superscript t stands for *true*, and $\Delta x_i$ and $\Delta y_i$ are random variables corresponding to errors associated with the measurement of individual probe positions, and $\Delta x_i^{\mathrm{o}}$ and $\Delta y_i^{\mathrm{o}}$ represent the *overlay* error introduced when the probe images are combined to produce a single image for distance measurements (see figure 1 (c)). Note that it is sufficient to include the overlay error only for one of the probes. In the experimental study by Koyama et al. [15] it was demonstrated that the statistics of $\Delta u_i^{(\mathrm{o})}$, where $u \in \{x, y\}$, can be well described by uncorrelated Gaussian distributions with zero mean and standard deviation $\sigma_{u,i}^{(\mathrm{o})}$. Therefore, the square of the measured distance between the probes is a random variable given by $R^2 = (\mu_x + \Delta x_1 - \Delta x_2 + \Delta x^{\mathrm{o}})^2 + (\mu_y + \Delta y_1 - \Delta y_2 + \Delta y^{\mathrm{o}})^2$, where $\mu_u = |u_1^{\mathrm{t}} - u_2^{\mathrm{t}}|$, $u \in \{x, y\}$. Let $X$ and $Y$ be Gaussian random variables with mean and variance $\mu_U = \mu_u$, $\sigma_U^2 = \sigma_{\Delta u_1}^2 + \sigma_{\Delta u_2}^2 + \sigma_{\Delta u^o}^2$, where $U \in \{X, Y\}$ and $u \in \{x, y\}$. We note that $R^2 = \sigma_X^2 \left(X/\sigma_X\right)^2 + \sigma_Y^2 \left(Y/\sigma_Y\right)^2$ is a sum of two chi-squared random variables with non-zero means [17], whose distribution is given by the convolution of two chi-squared distributions with different means and variances, and can be expressed as

$$f_{R^2}(z|\mu_X, \mu_Y) = \frac{\sqrt{z\mu_X\mu_Y}}{4{\sigma_X}^2{\sigma_Y}^2} e^{-\left(\mu_X^2\sigma_X^{-2} + \mu_Y^2\sigma_Y^{-2}\right)/2} \times \int_0^1 dw \frac{I_{-\frac{1}{2}}\left(\mu_X\sigma_X^{-2}\sqrt{zw}\right) I_{-\frac{1}{2}}\left(\mu_Y\sigma_Y^{-2}\sqrt{z(1-w)}\right)}{\left(w(1-w)\right)^{1/4} e^{z\left(w\sigma_X^{-2} + (1-w)\sigma_Y^{-2}\right)/2}}. \tag{18}$$

When $\sigma_X = \sigma_Y = \sigma$, this result reduces to

$$f_{R^2}(z|d) = \left(2\sigma^2\right)^{-1} e^{-(z+d^2)/2\sigma^2} I_0\left(d\sigma^{-2}\sqrt{z}\right), \tag{19}$$

where $d = \sqrt{\mu_X^2 + \mu_Y^2}$ is the true distance between the probes. As we considered spherically symmetric solutions of the Smoluchowski equation, the Green's function

obtained in this study allows us to only consider the case where the error in $x$ and $y$ directions are equal in magnitude. We should note that experimental observations often indicate that error in orthogonal directions are of comparable magnitude [15]. Assuming that the error in $x$ and $y$ directions have the same magnitude enables us to use our Green's functions that are given in polar coordinates, and express the probability that the probes will be colocalized at time $t$, denoted by $P_{\rm clc}(t|r_0)$, by

$$P_{\rm clc}(t|r_0) = 2\pi \int_0^{L^2} dz \int_a^b dr f_{R^2}(z|r) r \rho(r,t) + [1 - S(t)] \int_0^{L^2} dz f_{R^2}(z|a), \tag{20}$$

where $S(t)$ is the survival probability given in equation (4).

If the particle is initially bound to the reaction center, we can use equation (17) to calculate the probability with which the probes look colocalized at time $t$, denoted by $P_{\rm clc}(t|*)$, which yields

$$P_{\rm clc}(t|*) = 2\pi \int_0^{L^2} dz \int_a^b dr f_{R^2}(z|r) r \rho_\ell(r) + [1 - S(t|*)] \int_0^{L^2} dz f_{R^2}(z|a), \tag{21}$$

where $S(t|*)$ is equal to the integral of $\rho(r,t|*)$ (see equation (17)) over all space.

Note that $P_{\rm clc}(t)$ (regardless of the initial condition) is the probability that the probes will look colocalized at time $t$ given the threshold $L$ and uncertainty $\sigma$, whether the probes are actually bound or not.

In order to display the behavior of $P_{\rm clc}(t|r_0)$ and $P_{\rm clc}(t|*)$, we consider the case in which a molecule reversibly binds to a fixed reaction center at $r = a$ in a circular domain of radius $b$ with reflective boundaries. Two different initial conditions are employed: one for which an average over all initial positions $r_0 \in (a, b)$ is carried out, as initial conditions are usually not accessible, and another where we consider an initially bound pair. In the biological context, the fixed reaction center may correspond to a temporarily immobilized signaling platform that can reversibly recruit secondary molecules [18], and the confining domain may be induced by the membrane skeleton [19], or other membrane domains [20].

In figures 3-5, we plot the colocalization probabilities calculated by equations (20) and (21) to explore the effects of the magnitude of the measurement uncertainty $\sigma$, colocalization threshold $L$, and the effective rate parameters $k_{\rm r}$ and $k_{\rm d}$. All plots in figures 3, 4, and 5 are based on the same parameter values for $D$, $a$, and $b$, which are: $D = 8\ \mu{\rm m}^{-2}{\rm s}^{-1}$, a typical value estimated for diffusion in the plasma membrane of live cells at microsecond timescale [19], $a = 4$ nm, which is approximately the sum of the radii of two proteins, and $b = 200$ nm that we chose to consider a sub-micron confining domain. We frequently consider $\sigma = 45$ nm and $L = 100$ nm, which are representative values of position uncertainity and colocalization threshold in current single particle/molecule tracking experiments [15].

In all panels of figure 3, colocalization probability for an initially unbound pair is displayed as a function of time. All curves are obtained from equation (20), by considering a reflective boundary at $r = b$, and averaging over all initial positions. In figure 3(a-d), $P_{\rm clc}(t)$ vs time is plotted for three different values of $\sigma$, and each panel

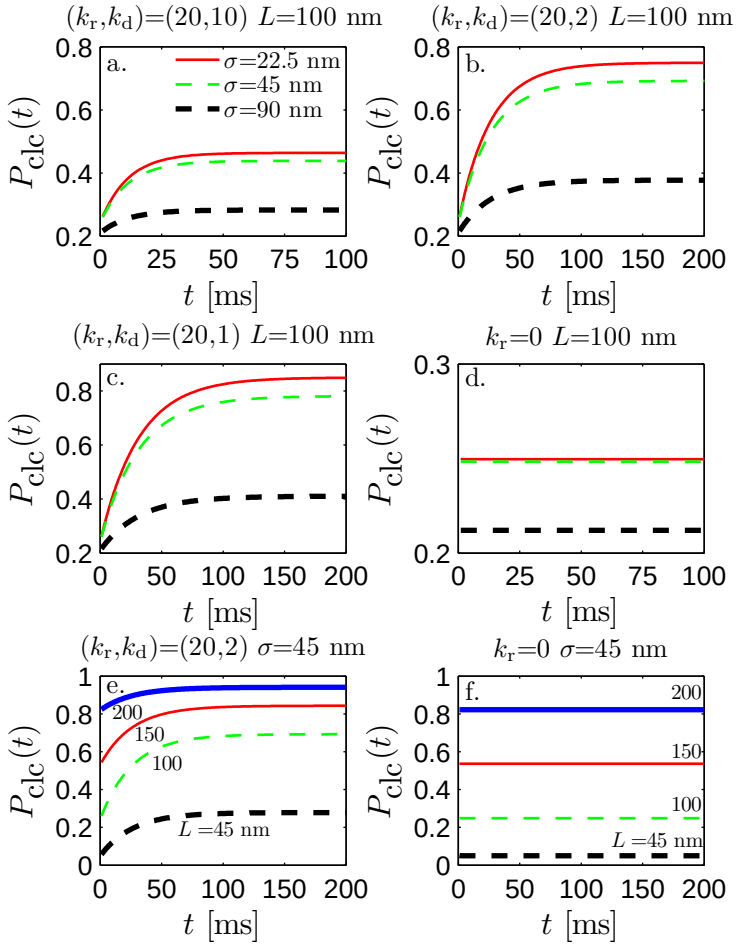


**Figure 3.** Colocalization probability averaged over all (unbound) initial conditions, $P_{\rm clc}(t)$, as a function of time, displayed for different values of the measurement uncertainty $\sigma$, colocalization threshold $L$, and the pair ($k_{\rm r}$, $k_{\rm d}$). $P_{\rm clc}(t)$ is obtained by evaluating equation (20) with reflective boundary conditions, and averaging over all initial positions. In all plots, we considered $D = 8$ $\mu$m$^{-2}$s$^{-1}$ (diffusion coefficient), $a = 4$ nm, and $b = 200$. In plots **a-d**, we display $P_{\rm clc}(t)$ vs $t$, for three different values of the measurement uncertainty, such that $\sigma$ = 22.5 nm (solid red), 45 nm (dashed green), 90 nm (dashed thick), and the value of $L$ is fixed at 100 nm. Values of the effective forward and backward rates, shown by using the notation ($k_{\rm r}$, $k_{\rm d}$), where $k_{\rm r}$ and $k_{\rm d}$ are in units of $\mu$m$^{-1}$ and $\mu$m$^{-2}$, respectively, but the units will be omitted for brevity in notation, vary through **a-d**, and are equal to (20,10) (**a**), (20,2) (**b**), (20,1) (**c**), such that the dissociation rate decreases as we go from **a** to **c**. In **d**, we have $k_{\rm r}$ = 0, corresponding to a non-reactive system. We chose the value $k_{\rm r}$ = 20 $\mu$m$^{-1}$ arbitrarily, and the choices $k_{\rm d}$ =10, 2, 1 $\mu$m$^{-2}$ correspond to average dissociation times of $k_{\rm d}'^{-1} = (Dk_{\rm d})^{-1}$ of 12.5, 62.5, and 125 ms, respectively. In **e-f**, $P_{\rm clc}(t)$ vs $t$ is shown for different values of the colocalization threshold $L$, by keeping the value $\sigma$ =45 nm fixed. We consider a reactive system in **e**, with ($k_{\rm r}$, $k_{\rm d}$)=(20,2), whereas **f** corresponds to the case of no reaction. In both plots, different curves correspond to different values of $L$, such that $L$=200 nm (thick solid blue), 150 nm (solid red), 100 nm (dashed green), 45 nm (thick dashed black).

corresponds to a different value of the effective rate ($k_r$,$k_d$), such that ($k_r$,$k_d$)=(20,10) (**a**), (20,2) (**b**), (20,1) (**c**), and panel (**d**) corresponds to a non-reactive system where $k_r = 0$. Note that $k_r$, and $k_d$ are in units of $\mu m^{-1}$ and $\mu m^{-2}$, respectively. However, for brevity, we will omit the units while using the notation ($k_r$, $k_d$) throughout the text and figure captions. In panels **a-c**, we used an arbitrary nonzero value for $k_r$, which is 20 $\mu m^{-1}$, and varied the effective dissociation rate $k_d$. Note that the choices $k_d$ =10, 2, 1 $\mu m^{-2}$ correspond to average dissociation times of $k_d'^{-1} = (Dk_d)^{-1}$ of 12.5, 62.5, and 125 ms, respectively, and are comparable with recent experimental findings [21]. In order to show the effects of measurement uncertainty, in panels **a-d**, we plotted $P_{clc}(t)$ for three different values of $\sigma$: $\sigma$ = 22.5 nm (solid red line), 45 nm (dashed green line), 90 nm (dashed thick line), while fixing the value of $L$ at 100 nm. Note that $\sigma$ affects both the transient behavior and the asymptotic value of colocalization probability, suggesting that it is essential to quantitatively account for measurement uncertainties while interpreting the outcomes of single particle/molecule tracking experiments. Our results also suggest that improving the precision with which probe positions are measured may or may not have a strong effect on the time-dependent colocalization probability depending on how much precision one is already working with. With the parameter values we considered here, one can see in figure 3(**a-d**) that decreasing the measurement uncertainty from 90 nm to 45 nm has a much more dramatic effect than reducing it further from 45 nm to 22.5 nm. Finally, the colocalization probabilities in **a-c** are higher than those in **d**, where the particle does not bind to the reaction center at all, as expected. In panels **e** and **f** of figure 3, we display the effect of $L$, for a fixed value of $\sigma$, $\sigma$ = 45 nm. In **e**, we consider a reactive system with ($k_r$, $k_d$)=(20,2), whereas in **f**, there is no possibility of reaction, i.e. $k_r = 0$. In both plots, different curves correspond to different values of $L$, such that $L$=200 nm (thick solid blue), 150 nm (solid red), 100 nm (dashed green), 45 nm (thick dashed black). Note that asyptotic colocalization probabilities are lower in **f**, as compared to **e**, due to the absence of interactions. As a final remark, we would like to mention that finding the optimal value of $L$ would depend on other parameters including particle density and bleaching time of fluorescent dyes, where the latter also affects the maximum possible length of particle trajectories, limiting the size of data sets from which colocalization probability is calculated.

In figure 4, we show the results of the same analysis as we described above, but for a probe that is initially bound to the target, and keeps undergoing reversible reactions with the target after a dissociation takes place. In this case, we use equation (21) and again consider a reflective boundary at $r = b$. The interpretation of results shown in figure 4 are very similar to those in figure 3 we discussed above, with the only significant difference being the colocalization probability decreasing as function of time, as one would expect for an initially bound pair.

Lastly, we include figure 5 to demonstrate the behavior of colocalization probability as a function of time, for different values of ($k_r$, $k_d$) where the ratio $k_r/k_d$ is constant. That is, we consider cases where the steady state is the same (see equation (15)), but the kinetics is quite different. In panel **a** and **b**, we display plots of $P_{clc}(t)$ and $P_{clc}(t|*)$,

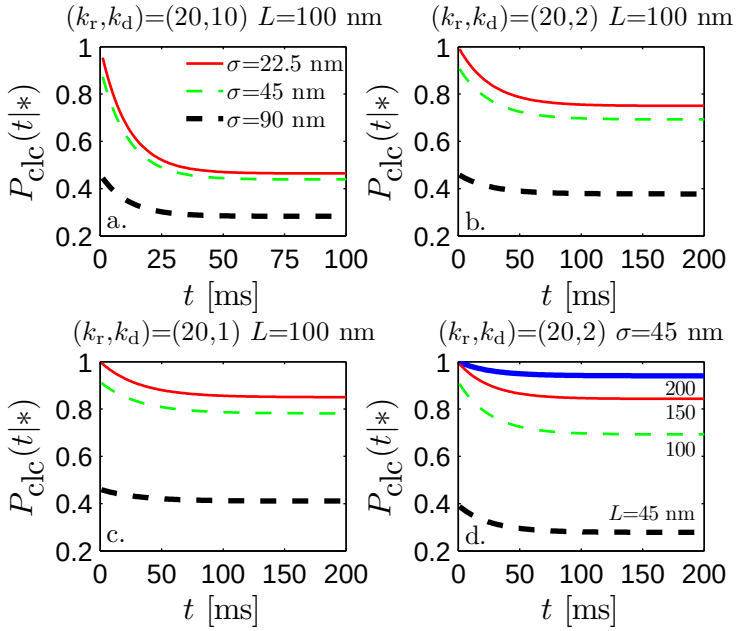


**Figure 4.** Colocalization probability for an initially bound pair, $P_{\rm clc}(t|*)$, as a function of time, shown for different values of the measurement uncertainty $\sigma$, colocalization threshold $L$, and the pair ($k_{\rm r}$, $k_{\rm d}$). $P_{\rm clc}(t|*)$ is obtained by evaluating equation (21) with a reflective boundary condition at $r = b$. In all plots, we used the parameter values: $D = 8\ \mu{\rm m}^{-2}{\rm s}^{-1}$ (diffusion coefficient), $a = 4$ nm, $b = 200$ nm. In **a-c**, we display $P_{\rm clc}(t|*)$ vs $t$, for three different values of the measurement uncertainty, such that $\sigma = 22.5$ nm (solid red), 45 nm (dashed green), 90 nm (dashed thick), and the value of $L$ is fixed at 100 nm. As in figure 3, values of the effective forward and backward rates, shown by using the notation ($k_{\rm r}$, $k_{\rm d}$), where $k_{\rm r}$ and $k_{\rm d}$ are in units of $\mu{\rm m}^{-1}$ and $\mu{\rm m}^{-2}$, respectively, but the units will be omitted for brevity in notation, vary through **a-c**, and are equal to (20,10) (**a**), (20,2) (**b**), (20,1) (**c**), such that the dissociation rate decreases as we go from **a** to **c**. We chose the value $k_{\rm r} = 20\ \mu{\rm m}^{-1}$ arbitrarily, and the choices $k_{\rm d}$ =10, 2, 1 $\mu{\rm m}^{-2}$ correspond to average dissociation times of $k_{\rm d}'^{-1} = (Dk_{\rm d})^{-1}$ of 12.5, 62.5, and 125 ms, respectively. In **d**, $P_{\rm clc}(t|*)$ vs $t$ is shown for different values of the colocalization threshold $L$, by keeping the value $\sigma$ =45 nm fixed, for a reactive system with ($k_{\rm r}$, $k_{\rm d}$)=(20,2). In **d**, different curves correspond to different values of $L$, such that $L$=200 nm (thick solid blue), 150 nm (solid red), 100 nm (dashed green), 45 nm (thick dashed black).

respectively, thus covering both initially unbound and bound states. In both panels, different curves correspond to different values of ($k_{\rm r}$, $k_{\rm d}$), that are: ($k_{\rm r}$, $k_{\rm d}$)=(250,125) (solid blue), (50,25) (dashed red), (10,5) (thick dashed green), (2,1) (thick solid black), where the color or line style coding is the same between the panels. We again chose the values of $k_{\rm r}$ arbitrarily as in figure 3, and the choices $k_{\rm d}$ =125, 25, 5, 1 $\mu{\rm m}^{-2}$ correspond to average dissociation times of $k_{\rm d}'^{-1} = (Dk_{\rm d})^{-1}$ of 1, 5, 25, and 125 ms, respectively. Note that the duration of the transient is proportional to the average dissociation time, as one would expect intuitively. In practical applications, unless the frame time is sufficiently short, it can be difficult to distinguish cases with the same steady state, but with very different kinetics. We believe that ours and similar calculations could be

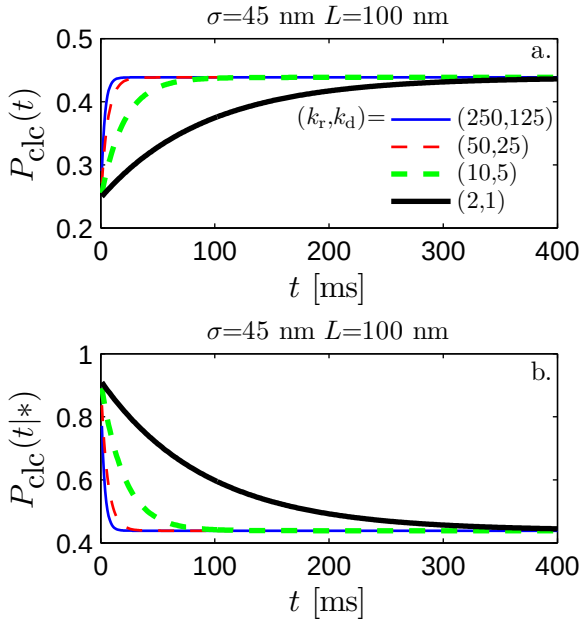


**Figure 5.** Colocalization probability for initially unbound and bound pairs as a function of time, shown for different values of the the pair ($k_{\rm r}$, $k_{\rm d}$), while the ratio $k_{\rm r}/k_{\rm d}$ is a constant. In both plots, we used the parameter values: diffusion coefficient $D = 8\ \mu{\rm m}^{-2}{\rm s}^{-1}$, $a = 4$ nm, $b = 200$ nm, measurement uncertainty $\sigma$ =45 nm, and colocalization threshold $L = 100$ nm. In **a**, we display the behavior of $P_{\rm clc}(t)$, colocalization probability for an unbound pair, vs $t$, obtained by evaluating equation (20) with reflective boundary conditions. In **b**, we plot $P_{\rm clc}(t|*)$, colocalization probability for an initially bound pair, vs $t$, obtained via equation (21) with reflective boundary conditions. In both plots, different curves correspond to different values of ($k_{\rm r}$, $k_{\rm d}$), where $k_{\rm r}$ and $k_{\rm d}$ are in units of $\mu{\rm m}^{-1}$ and $\mu{\rm m}^{-2}$, respectively, but the units will be omitted for brevity in notation, and are equal to (250,125) (solid blue), (50,25) (dashed red), (10,5) (thick dashed green), (2,1) (thick solid black). We chose the values of $k_{\rm r}$ arbitrarily, and the choices $k_{\rm d}$ =125, 25, 5, 1 $\mu{\rm m}^{-2}$ correspond to average dissociation times of $k_{\rm d}'^{-1} = (Dk_{\rm d})^{-1}$ of 1, 5, 25, and 125 ms, respectively.

useful in predicting how short the frame time should be in order to reliably investigate molecular interactions via single particle/molecule tracking techniques.

Before we finish this section, we would like to note that there is one more source of position uncertainty that we did not account for in the calculations above, which due to the *detector time averaging* effect [22]. In single particle/molecule tracking experiments, the camera obtains images by collecting photons from a probe for an extended period of time. This *measurement time* can be less than or equal to the time between two observations, i.e. the *frame time*. Therefore, if a probe moves during the measurement time, its observed position will reflect the average position of the probe rather than its actual position at that moment in time. As shown previously [22], this effect could be significant, and should be accounted for in more detailed treatments of this problem. In order to obtain analytical results about this aspect of the problem, we need to consider the probe position averaged over the measurement time as the random position variable,

given by

$$\bar{\vec{r}}(n) = \int_{n\Delta t}^{(n+1)\Delta t} dt \vec{r}(t), \tag{22}$$

where $\Delta t$ is the measurement time, which is taken to be equal to the frame time, and $n$ is the frame number. In principle, one may calculate the distribution of $\bar{\vec{r}}(n)$ through

$$f(\vec{R}, n) = \left\langle \delta\left(\vec{R} - \bar{\vec{r}}(n)\right)\right\rangle, \tag{23}$$

where the angular brackets correspond to an average over all possible realizations of $\vec{r}(t)$, and $\delta(\vec{R} - \vec{R}_0)$ denotes the Dirac-delta distribution centered at $\vec{R}_0$.

## 4. Discussion and Conclusions

In summary, we presented exact Green's functions for a Brownian particle reversibly reacting with a fixed target in a finite 2D disc with reflective or absorbing boundaries considering spherically symmetric initial conditions, or an initially bound particle-target pair. To our knowledge, this is the first time these results are given in a 2D space. Therefore, our study also fills the gap between the known solutions in 1D [9] and 3D (unbounded space) [10]. As we argue below, our theoretical results can be useful in several different contexts.

In contrast to diffusion limited reactions in unbounded 3D space, asymptotic value of the reaction rate in 2D was shown to be zero, and this was attributed to the insufficient flux of reactants in 2D that cannot sustain a steady reaction rate [11]. However, it is possible to talk about a non-zero reaction rate in 2D as long as the reactants are confined to a finite region of space. In this respect, we hope that the result given here for a domain with reflective boundaries will be useful in interpreting future experimental data for reacting particles trapped in a confining domain.

To demonstrate a potential application of the Green's functions given here, we calculated the effect of measurement procedures on the outcome of single particle/molecule tracking experiments conducted to investigate molecular interactions in surfaces such as the plasma membrane of live cells (see figure 3), based on a common scheme of modelling measurement uncertainties [15]. Imaging techniques that are suitable for observing the dynamics of single particles/molecules all suffer from the presence of an uncertainty in determining the position of a fluorescent molecule. This uncertainty stems from the use of diffraction limited optics, overlaying of different images, noise from detector electronics, etc. and impairs the measurement of distance between interacting molecules [15, 16, 21]. Even though we dealt with a spherically symmetric case, in this article, we addressed some of these problems by calculating the influence of finite precision of position measurements on the probability of colocalization as a function of time (also see figures 3-5), a quantity that can be measured. As we remarked at the end of section 3, in this work, we did not give explicit results on the detector time averaging effect. Nevertheless, we briefly outlined one of the ways of solving this problem while closing section 3, and we would like to address this issue

in our future work to provide a better prediction for the time-dependent colocalization probability, and in many other relevant problems.

Finally, we would like to comment on the computational study of a system of reactive Brownian particles, which attracts a great deal of attention and resulted in the production of many general-purpose simulation packages such as Brownmove [23, 24] ChemCell [25], Smoldyn [26], MCell [27], STOCHSIM [28]. We believe that our solution for the case of absorbing boundaries can be useful in performing Green's function reaction dynamics simulations [12, 13, 29]. In this semi-analytical simulation method, one needs to calculate the first arrival time of Brownian particles on the surface of *protective domains* that are employed to reduce the many body problem to a number of independent two-body problems. The first arrival problem can be solved by assuming an absorbing boundary at the target surface [30]. In this respect, our Green's functions can be employed to perform numerically exact simulations of reversibly reacting Brownian particles.

## 5. Acknowledgments

The author thanks Dr. Akihiro Kusumi and members of his laboratory for inspiring discussions on single molecule observations, and two anonymous reviewers for valuable comments. Thanks to Ikumi for her support and endless patience. This work was financially supported by World Premier International Research Center Initiative (WPI), Ministry of Education, Culture, Sports, Science and Technology (MEXT), Japan.

## Appendix A. Solution of the Smoluchowski equation in 2D with the back-reaction boundary condition and spherically symmetric initial distributions

### *Appendix A.1. Solution inside an annular domain with reflective outer boundary*

Suppose that the particles U and N undergo reversible dimerization, i.e. U+N↔UN with the forward rate $k'_{\mathrm{r}}$ when the distance between them is equal to $a$, and the product UN dissociates with rate $k'_{\mathrm{d}}$. If one of these particles is fixed, the other is a Brownian particle, and the space is isotropic and homogeneous the probability density $\rho(r,t)$ for the distance between these particles at time $t$ will evolve according to

$$\frac{\partial \rho}{\partial t} = D\frac{1}{r}\frac{\partial}{\partial r}\left(r\frac{\partial \rho}{\partial r}\right), \tag{A.1}$$

where $D$ is the diffusion coefficient of the mobile particle. The boundary conditions are chosen such that at $r = a$ reaction or dissociation occurs, and at a greater distance $b$ the molecules are reflected. The reflective boundary condition is considered to study the effects of confinement on reaction kinetics. We make the following definitions for brevity in notation

$$s = Dt,$$

$$k_{\mathrm{r}} = \frac{k'_{\mathrm{r}}}{2\pi Da},$$
$$k_{\mathrm{d}} = \frac{k'_{\mathrm{d}}}{D}.$$

The boundary conditions and the initial condition are given by

$$2\pi aD \left.\frac{\partial \rho(r,s)}{\partial r}\right|_{r=a} = 2\pi aDk_{\mathrm{r}}\rho(a,s) - Dk_{\mathrm{d}}\left(1 - S(s)\right), \tag{A.2}$$

$$\left.\frac{\partial \rho(r,s)}{\partial r}\right|_{r=b} = 0, \tag{A.3}$$

$$\rho(r,0) = \frac{\delta(r-r_0)}{2\pi r_0}, \tag{A.4}$$

where equation (A.2) is the so called *back reaction* boundary condition [9, 10], $S(s)$ is the probability that the particles are not bound at $s$, given the initial condition in equation (A.4), and is expressed by

$$S(s) = 1 - 2\pi a \int_0^s du \left.\frac{\partial \rho(u,r)}{\partial r}\right|_{r=a}. \tag{A.5}$$

Substituting the above expression for $S(s)$, equation (A.2) reads

$$\left.\frac{\partial \rho(r,s)}{\partial r}\right|_{r=a} = k_{\mathrm{r}}\rho(a,s) - k_{\mathrm{d}} \int_0^s du \left.\frac{\partial \rho(r,u)}{\partial r}\right|_{r=a}. \tag{A.6}$$

The solution of equation (A.1) together with the boundary conditions and the initial condition given in equations (A.3,A.4) and (A.6) can be expressed as

$$\rho(r,s) = G^{(1)}(r,s|r_0,0) + f(r,s), \tag{A.7}$$

where $G^{(1)}(r,s|r_0,0)$ is the Green's function for equation (A.1) with reflective boundaries at $r=a$ and $r=b$, and $f(r,s)$ is a function that satisfies the boundary conditions and vanishes everywhere at $s=0$. The form of $G^{(1)}(r,s|r_0,0)$ is well known [14], and is explicitly given by

$$\begin{aligned} G^{(1)}(r,s|r_0,0) &= \frac{1}{\pi(b^2-a^2)} + \frac{\pi}{4}\sum_{n=1}^{\infty} \frac{J_1^2(b\alpha_n)}{F(\alpha_n)} C_0(r,\alpha_n)C_0(r_0,\alpha_n)e^{-\alpha_n^2 s} \\ &= \frac{1}{\pi(b^2-a^2)} + \sum_{n=1}^{\infty} g_n^{(1)}(r|r_0)e^{-\alpha_n^2 s}. \end{aligned} \tag{A.8}$$

where $\alpha_n$'s are the positive roots of

$$J_1(a\alpha)Y_1(b\alpha) - Y_1(a\alpha)J_1(b\alpha) = 0, \tag{A.9}$$

and $F(\alpha_n)$ and $C_0(r,\alpha_n)$ are given by

$$F(\alpha_n) = \left[J_1^2(a\alpha_n) - J_1^2(b\alpha_n)\right], \tag{A.10}$$

$$C_0(r,\alpha_n) = \alpha_n\left[J_0(r\alpha_n)Y_1(a\alpha_n) - Y_0(r\alpha_n)J_1(a\alpha_n)\right]. \tag{A.11}$$

In order to obtain the function $f(r,s)$, we need to solve equation (A.1) with the boundary conditions given in equations (A.3) and (A.6). Here we use Laplace transform

to reduce equation (A.1) to an ordinary differential equation. Taking the Laplace transforms of equations (A.1,A.3) and (A.6), we obtain the ordinary differential equation

$$\frac{d^2\widetilde{f}(r,\epsilon)}{dr^2}+\frac{1}{r}\frac{d\widetilde{f}(r,\epsilon)}{dr}-\epsilon\widetilde{f}(r,\epsilon)=0, \tag{A.12}$$

as $f(r,0)=0$, with the boundary conditions

$$\left.\frac{\partial\widetilde{f}(r,\epsilon)}{\partial r}\right|_{r=a}=\frac{\epsilon k_r}{\epsilon+k_d}\left[\widetilde{G}^{(1)}(a,\epsilon|r_0,0)+\widetilde{f}(a,\epsilon)\right], \tag{A.13}$$

$$\left.\frac{\partial\widetilde{f}(r,\epsilon)}{\partial r}\right|_{r=b}=0. \tag{A.14}$$

equation (A.12) is the well-known modified Bessel differential equation whose solution is

$$\widetilde{f}(r,\epsilon)=AI_0(r\omega)+BK_0(r\omega), \tag{A.15}$$

where $\omega=\sqrt{\epsilon}$, and $I_0(x)$ and $K_0(x)$ are modified Bessel functions of order zero, of the first and second kind, respectively. The integration constants $A$ and $B$ are found by imposing the boundary conditions. Substituting the formal solution given by equation (A.15) in equations (A.14) and (A.13), we get a system of equations for $A$ and $B$

$$\begin{bmatrix} I_1(b\omega) & -K_1(b\omega) \\ I_1(a\omega)-\omega' I_0(a\omega) & -K_1(a\omega)-\omega' K_0(a\omega) \end{bmatrix}\begin{bmatrix} A \\ B \end{bmatrix}=\begin{bmatrix} 0 \\ \omega'\widetilde{G}^{(1)}(a,\omega|r_0) \end{bmatrix}, \tag{A.16}$$

where $\omega'=\omega k_{\rm r}/(\omega^2+k_{\rm d})$. Solving for $A$ and $B$, we obtain

$$A(\omega)=-\omega k_{\rm r}\widetilde{G}^{(1)}(a,\omega|r_0)K_1(b\omega)\Big[\left(\omega^2+k_{\rm d}\right)\left[I_1(b\omega)K_1(a\omega)-I_1(a\omega)K_1(b\omega)\right] + \omega k_{\rm r}\left[I_1(b\omega)K_0(a\omega)+I_0(a\omega)K_1(b\omega)\right]\Big]^{-1},$$

$$B(\omega)=I_1(b\omega)\frac{A(\omega)}{K_1(b\omega)},$$

Therefore, the full solution becomes

$$\widetilde{\rho}(r,\omega)=\widetilde{G}^{(1)}(r,\omega|r_0)+\widetilde{f}(r,\omega), \tag{A.17}$$

$$\widetilde{f}(r,\omega)=A(\omega)\left[I_0(r\omega)+\frac{K_0(r\omega)I_1(b\omega)}{K_1(b\omega)}\right] \tag{A.18}$$

With the knowledge of the solution in the Laplace domain, we can immediately calculate the asymptotic distribution of $r$. Using the final value theorem for the Laplace transform, we obtain

$$\lim_{s\to\infty}\rho(r,s)=\lim_{\epsilon\to 0}\epsilon\widetilde{\rho}(r,\epsilon)=\frac{1}{\pi(b^2-a^2)+2\pi a k_{\rm r}/k_{\rm d}}. \tag{A.19}$$

In order to find the solution in time domain, we need to be able to take the inverse Laplace transform of the second term in the equation above. By using the convolution theorem for the Laplace transform, we can write

$$f(r,s)=-k_{\rm r}\int_0^s duG^{(1)}(r,s-u|r_0,0)\mathcal{L}^{-1}\Big\{\omega\left[K_1(b\omega)/C_1(\omega)\right]I_0(r\omega) + \omega\left[I_1(b\omega)/C_1(\omega)\right]K_0(r\omega)\Big\}(u), \tag{A.20}$$

where $\mathcal{L}^{-1}$ is the inverse Laplace transformation operator defined as

$$g(s) = \mathcal{L}^{-1}\left\{\widetilde{g}(\epsilon)\right\}(s) = \frac{1}{2\pi i}\int_{\xi-i\infty}^{\xi+i\infty} d\epsilon e^{\epsilon s}\widetilde{g}(\epsilon), \tag{A.21}$$

in which $\xi$ is a real number larger than the real part of the right-most singularity of $\widetilde{g}$, and

$$\begin{aligned} C_1(\omega) = &\left(\omega^2 + k_\mathrm{d}\right)\left[I_1(b\omega)K_1(a\omega) - I_1(a\omega)K_1(b\omega)\right] \\ &+ \omega k_\mathrm{r}\left[I_1(b\omega)K_0(a\omega) + I_0(a\omega)K_1(b\omega)\right]. \end{aligned} \tag{A.22}$$

Hence, we need to perform an integral of the form

$$\mathcal{I} = \frac{1}{2\pi i}\int_{\gamma-i\infty}^{\gamma+i\infty} d\epsilon e^{\epsilon s}\sqrt{\epsilon}\frac{K_1(b\sqrt{\epsilon})I_0(r\sqrt{\epsilon}) + I_1(b\sqrt{\epsilon})K_0(r\sqrt{\epsilon})}{C_1(\sqrt{\epsilon})}, \tag{A.23}$$

To evaluate this contour integral, we investigate the location of the integrand's singularities. First of all, in the limit $\epsilon \to 0$, the integrand remains finite, with the following limit

$$\lim_{\epsilon\to 0} e^{\epsilon s}\sqrt{\epsilon}\frac{K_1(b\sqrt{\epsilon})I_0(r\sqrt{\epsilon}) + I_1(b\sqrt{\epsilon})K_0(r\sqrt{\epsilon})}{C_1(\sqrt{\epsilon})} = -\frac{2a}{k_\mathrm{d}(a^2-b^2) - 2ak_\mathrm{r}}, \tag{A.24}$$

which was used to obtain equation (A.19). A closer inspection of the integrand reveals that is has simple poles along the negative $x$-axis. Finally, $f(r,s)$ can be expressed as

$$\begin{aligned} f(r,s) = &-k_\mathrm{r}\int_0^s du G^{(1)}(r, s-u|r_0, 0) \\ &\times \sum_{n=1}^{\infty} e^{-\omega_n^2 s} i\omega_n \frac{K_1(ib\omega_n)I_0(ir\omega_n) + I_1(ib\omega_n)K_0(ir\omega_n)}{C_1'(i\omega_n)}, \end{aligned} \tag{A.25}$$

where $C_1' = dC_1/d\epsilon$, and $\omega_n$ are the real and positive roots of $C_1(i\omega)$, which is given by

$$\begin{aligned} C_1(i\omega) = &\pi\frac{k_\mathrm{d}-\omega^2}{2}\left[J_1(a\omega)Y_1(b\omega) - J_1(b\omega)Y_1(a\omega)\right] \\ &- \pi\frac{k_\mathrm{r}\omega}{2}\left[J_0(a\omega)Y_1(b\omega) - J_1(b\omega)Y_0(a\omega)\right]. \end{aligned} \tag{A.26}$$

After expressing the modified Bessel functions with imaginary arguments as a combination of Bessel functions of the first kind, we obtain

$$\begin{aligned} f(r,s) = &\pi k_\mathrm{r}\int_0^s du G^{(1)}(r, s-u|r_0, 0) \\ &\times \sum_{n=1}^{\infty} e^{-\omega_n^2 s} \omega_n \frac{Y_1(b\omega_n)J_0(r\omega_n) - J_1(b\omega_n)Y_0(r\omega_n)}{2C_1'(i\omega_n)}, \end{aligned} \tag{A.27}$$

where

$$\begin{aligned} C_1'(i\omega) = &-\pi\frac{J_1(a\omega)}{4\omega}\left[b\left(k_\mathrm{d}-\omega^2\right)Y_0(b\omega) - \frac{2k_\mathrm{d} - ak_\mathrm{r}\omega^2}{\omega}Y_1(b\omega)\right] \\ &+ \frac{\pi J_1(b\omega)}{4\omega}\left[a\left(k_\mathrm{d}-\omega^2\right)Y_0(a\omega) - \frac{2k_\mathrm{d} - ak_\mathrm{r}\omega^2}{\omega}Y_1(a\omega)\right] \\ &+ \frac{\pi J_0(a\omega)}{4}\left[bk_\mathrm{r}Y_0(b\omega) - a\frac{k_\mathrm{d}-\omega^2}{\omega}Y_1(b\omega)\right] \\ &- \frac{\pi J_0(b\omega)}{4}\left[bk_\mathrm{r}Y_0(a\omega) - b\frac{k_\mathrm{d}-\omega^2}{\omega}Y_1(a\omega)\right]. \end{aligned} \tag{A.28}$$

Finally, the solution as a function of time becomes

$$f(r,t) = k_{\mathrm{r}} \int_0^s du G^{(1)}(r, s-u|r_0, 0) \sum_{n=1}^{\infty} h_n^{(1)}(r) e^{-\omega_n^2 Dt}, \tag{A.29}$$

where

$$h_n^{(1)}(r) = \pi\omega_n \frac{Y_1(b\omega_n)J_0(r\omega_n) - J_1(b\omega_n)Y_0(r\omega_n)}{2C_1'(i\omega_n)}. \tag{A.30}$$

Therefore, the full solution becomes

$$\begin{aligned}\rho^{(1)}(r,t) = G^{(1)}(r,t|r_0,0) &+ \frac{k_{\mathrm{r}}}{\pi(b^2-a^2)} \sum_m h_m^{(1)}(r) \frac{1-e^{-\omega_m^2 Dt}}{\omega_m^2} \\ &+ k_{\mathrm{r}} \sum_{m,n} h_m^{(1)}(r) g_n^{(1)}(r|r_0) \frac{e^{-\omega_m^2 Dt} - e^{-\alpha_n^2 Dt}}{\alpha_n^2 - \omega_m^2},\end{aligned} \tag{A.31}$$

where we use the superscript (1) to indicate that this solution pertains to the domain with reflective outer boundary, to be consistent with the main text. Using equation (A.19), we deduce

$$\frac{k_{\mathrm{r}}}{\pi(b^2-a^2)} \sum_m \frac{h_m^{(1)}(r)}{\omega_m^2} = \begin{cases} \left[\pi(b^2-a^2) + 2\pi a k_{\mathrm{r}}/k_{\mathrm{d}}\right]^{-1} - \left[\pi(b^2-a^2)\right]^{-1}, & \text{for } k_{\mathrm{d}} > 0 \\ -\left[\pi(b^2-a^2)\right]^{-1}, & \text{for } k_{\mathrm{d}} = 0 \end{cases}$$

Therefore, we can write

$$\begin{aligned}\rho^{(1)}(r,t) = &\sum_n g_n^{(1)}(r|r_0) e^{-\alpha_n^2 Dt} - \frac{k_{\mathrm{r}}}{\pi(b^2-a^2)} \sum_m h_m^{(1)}(r) \frac{e^{-\omega_m^2 Dt}}{\omega_m^2} \\ &+ k_{\mathrm{r}} \sum_{m,n} h_m^{(1)}(r) g_n^{(1)}(r|r_0) \frac{e^{-\omega_m^2 Dt} - e^{-\alpha_n^2 Dt}}{\alpha_n^2 - \omega_m^2} \\ &+ \frac{1}{\pi(b^2-a^2) + 2\pi a k_{\mathrm{r}}/k_{\mathrm{d}}}.\end{aligned} \tag{A.32}$$

The distribution of $r$, averaged over a time window $[(\ell-1)\Delta t, \ell\Delta t]$, where $\ell = 1, 2, 3, ...$, is then given by

$$\begin{aligned}\rho_\ell^{(1)}(r) = \frac{1}{\Delta t}\int_{(\ell-1)\Delta t}^{\ell\Delta t} dt \rho^{(1)}(r,t) &= \sum_n g_n^{(1)}(r|r_0) \frac{e^{-\alpha_n^2(\ell-1)D\Delta t}\left[1 - e^{-\alpha_n^2 D\Delta t}\right]}{\alpha_n^2 D\Delta t} \\ &- \frac{k_{\mathrm{r}}}{\pi(b^2-a^2)} \sum_m h_m^{(1)}(r) \frac{e^{-\omega_n^2(\ell-1)D\Delta t}\left[1 - e^{-\omega_n^2 D\Delta t}\right]}{\omega_m^4 D\Delta t} \\ &+ k_{\mathrm{r}} \sum_{m,n} \frac{h_m^{(1)}(r) g_n^{(1)}(r|r_0)}{(\alpha_n^2 - \omega_m^2)\, D\Delta t} \Big\{ \omega_n^{-2} e^{-\omega_n^2(\ell-1)D\Delta t}\left[1 - e^{-\omega_n^2 D\Delta t}\right] \\ &- \alpha_n^{-2} e^{-\alpha_n^2(\ell-1)D\Delta t}\left[1 - e^{-\alpha_n^2 D\Delta t}\right] \Big\} + \frac{1}{\pi(b^2-a^2) + 2\pi a k_{\mathrm{r}}/k_{\mathrm{d}}}.\end{aligned} \tag{A.33}$$

The time integral of the derivative at $r = a$ is given by

$$\int_0^t du \left.\frac{\partial \rho^{(1)}(r,u)}{\partial r}\right|_{r=a} = k_{\mathrm{r}} \sum_n g_n^{(1)}(r|r_0) \frac{e^{-\alpha_n^2 Dt} - e^{-k_{\mathrm{d}} Dt}}{k_{\mathrm{d}} - \alpha_n^2}$$

$$
\begin{aligned}
&- \frac{k_{\mathrm{r}}^2}{\pi(b^2-a^2)} \sum_m h_m^{(1)}(r) \frac{e^{-\omega_m^2 Dt} - e^{-k_{\mathrm{d}} Dt}}{\omega_m^2 \left(k_{\mathrm{d}} - \omega_m^2\right)} \\
&+ k_{\mathrm{r}}^2 \sum_{m,n} \frac{h_m^{(1)}(r) g_n^{(1)}(r|r_0)}{\alpha_n^2 - \omega_m^2} \Big\{ \left(k_{\mathrm{d}} - \omega_m^2\right)^{-1} \left[e^{-\omega_m^2 Dt} - e^{-k_{\mathrm{d}} Dt}\right] \\
&- \left(k_{\mathrm{d}} - \alpha_n^2\right)^{-1} \left[e^{-\alpha_n^2 Dt} - e^{-k_{\mathrm{d}} Dt}\right] \Big\} \\
&+ \frac{(k_{\mathrm{r}}/k_{\mathrm{d}}) \left[1 - e^{-k_{\mathrm{d}} Dt}\right]}{\pi(b^2-a^2) + 2\pi a k_{\mathrm{r}}/k_{\mathrm{d}}}.
\end{aligned} \tag{A.34}
$$

In obtaining these results, we used the following identities [14]

$$
K_\theta(ze^{\pm i\pi/2}) = \pm \frac{i\pi}{2} e^{\mp i\pi\theta/2} \left[-J_\theta(z) \pm i Y_\theta(z)\right], \qquad I_\theta(ze^{\pm i\pi/2}) = e^{\pm i\pi\theta/2} J_\theta(z),
$$

*Appendix A.2. Solution inside an annular domain with absorbing outer boundary*

In this case, the Laplace transform of the boundary condition at $r = b$ is

$$
\widetilde{\rho}(b, \epsilon) = 0, \tag{A.35}
$$

while the boundary condition at $a = 0$ is the same as the previous case, given in equation (A.13). Again, the solution can be written as a sum in the following form

$$
\widetilde{\rho}(r, \epsilon) = \widetilde{G}^{(2)}(r, \epsilon|r_0, 0) + \widetilde{f}(r, \epsilon), \tag{A.36}
$$

where $\widetilde{G}^{(2)}(r, \epsilon|r_0, 0)$ is the Laplace transform of the Green's function of the diffusion equation that satisfies equations (A.13) and (A.35). The Green's function $G^{(2)}(r, s|r_0, 0)$ is well-known [14], and is given by

$$
G^{(2)}(r, s|r_0, 0) = \frac{\pi}{4} \sum_{n=1}^{\infty} \frac{J_0^2(b\beta_n)}{F_2(\beta_n)} C_0(r, \beta_n) C_0(r_0, \beta_n) e^{-\beta_n^2 s} = \sum_{n=1}^{\infty} g_n^{(2)}(r|r_0) e^{-\beta_n^2 s}, \tag{A.37}
$$

where $\beta_n$'s are the positive roots of

$$
-J_1(a\beta) Y_0(b\beta) + Y_1(a\beta) J_0(b\beta) = 0, \tag{A.38}
$$

and $F(\beta_n)$ and $C_0(r, \beta_n)$ are given by

$$
F(\beta_n) = \left[J_1^2(a\beta_n) - J_0^2(b\beta_n)\right], \tag{A.39}
$$

$$
C_0(r, \beta_n) = \beta_n \left[J_0(r\beta_n) Y_1(a\beta_n) - Y_0(r\beta_n) J_1(a\beta_n)\right]. \tag{A.40}
$$

Similar to the previous case, $\widetilde{f}(r, \epsilon)$ can be expressed by equation (A.15). This time, we get the following system of equations for $A$ and $B$

$$
\begin{bmatrix} I_0(b\omega) & K_0(b\omega) \\ I_1(a\omega) - \omega' I_0(a\omega) & -K_1(a\omega) - \omega' K_0(a\omega) \end{bmatrix} \begin{bmatrix} A \\ B \end{bmatrix} = \begin{bmatrix} 0 \\ \omega' \widetilde{G}^{(2)}(a, \omega|r_0) \end{bmatrix}, \tag{A.41}
$$

Solving for $A$ and $B$, we obtain

$$
\begin{aligned}
A(\omega) = \omega k_{\mathrm{r}} \widetilde{G}^{(2)}(a, \omega|r_0) K_0(b\omega) \Big[ &\left(\omega^2 + k_{\mathrm{d}}\right) \left[I_0(b\omega) K_1(a\omega) + I_1(a\omega) K_0(b\omega)\right] \\
&+ \omega k_{\mathrm{r}} \left[I_0(b\omega) K_0(a\omega) - I_0(a\omega) K_0(b\omega)\right] \Big]^{-1},
\end{aligned}
$$

$$
B(\omega) = -I_0(b\omega) \frac{A(\omega)}{K_0(b\omega)},
$$

Therefore, the full solution becomes

$$\widetilde{\rho}(r,\omega) = \widetilde{G}^{(2)}(r,\omega|r_0) + \widetilde{f}(r,\omega), \tag{A.42}$$

$$\widetilde{f}(r,\omega) = A(\omega)\left[I_0(r\omega) - \frac{K_0(r\omega)I_0(b\omega)}{K_0(b\omega)}\right]. \tag{A.43}$$

Using the final value theorem for the Laplace transform we obtain

$$\lim_{s\to\infty}\rho(r,s) = \lim_{\epsilon\to 0}\epsilon\widetilde{\rho}(r,\epsilon) = 0, \tag{A.44}$$

which is consistent with the fact that the steady state solution must vanish everywhere due to the presence of the absorbing boundary. By using the convolution theorem for the Laplace transform, we write

$$\begin{aligned} f(r,s) = k_{\mathrm{r}}\int_0^s du G^{(2)}(r,s-u|r_0,0)\mathcal{L}^{-1}\Big\{&\omega\left[K_0(b\omega)/C_2(\omega)\right]I_0(r\omega) \\ &- \omega\left[I_0(b\omega)/C_2(\omega)\right]K_0(r\omega)\Big\}(u), \end{aligned} \tag{A.45}$$

where

$$\begin{aligned} C_2(\omega) = &\left(\omega^2 + k_{\mathrm{d}}\right)\left[I_0(b\omega)K_1(a\omega) + I_1(a\omega)K_0(b\omega)\right] \\ &+ \omega k_{\mathrm{r}}\left[I_0(b\omega)K_0(a\omega) - I_0(a\omega)K_0(b\omega)\right]. \end{aligned} \tag{A.46}$$

Hence, we need to perform an integral of the form

$$\mathcal{I} = \frac{1}{2\pi i}\int_{\xi-i\infty}^{\xi+i\infty} d\epsilon e^{\epsilon s}\sqrt{\epsilon}\frac{K_0(b\sqrt{\epsilon})I_0(r\sqrt{\epsilon}) - I_0(b\sqrt{\epsilon})K_0(r\sqrt{\epsilon})}{C_2(\sqrt{\epsilon})}, \tag{A.47}$$

To evaluate this contour integral, we investigate the location of the integrand's singularities. In the limit $\epsilon \to 0$, the integrand remains finite

$$\lim_{\epsilon\to 0} e^{\epsilon s}\sqrt{\epsilon}\frac{K_0(b\sqrt{\epsilon})I_0(r\sqrt{\epsilon}) - I_0(b\sqrt{\epsilon})K_0(r\sqrt{\epsilon})}{C_2(\sqrt{\epsilon})} = 0. \tag{A.48}$$

A closer inspection of the integrand reveals that is has simple poles along the negative $x$-axis. Finally, $f(r,s)$ can be expressed as

$$\begin{aligned} f(r,s) = &\pi k_{\mathrm{r}}\int_0^s du G^{(2)}(r,s-u|r_0,0) \\ &\times\sum_{n=1}^{\infty} e^{-\gamma_n^2 s} i\gamma_n \frac{-Y_0(b\gamma_n)J_0(r\gamma_n) + J_0(b\gamma_n)Y_0(r\gamma_n)}{2C_2'(i\gamma_n)}, \end{aligned} \tag{A.49}$$

where $C_1' = dC_1/d\epsilon$, and $\gamma_n$ are the real and positive roots of $C_1(i\gamma)$,

$$\begin{aligned} C_2(i\gamma) = &i\pi\frac{k_{\mathrm{d}} - \gamma^2}{2}\left[J_0(b\gamma)Y_1(a\gamma) - J_1(a\gamma)Y_0(b\gamma)\right] \\ &- i\pi\frac{k_{\mathrm{r}}\gamma}{2}\left[J_0(b\gamma)Y_0(a\gamma) - J_0(a\gamma)Y_0(b\gamma)\right], \end{aligned} \tag{A.50}$$

and its derivative is explicitly expressed as

$$\begin{aligned} C_2'(i\gamma) = &-\frac{i\pi J_1(a\gamma)}{4\gamma^2}\left[\left(\gamma^2(-ak_{\mathrm{r}}+1) + k_{\mathrm{d}}\right)Y_0(b\gamma) + b\gamma\left(k_{\mathrm{d}} - \gamma^2\right)Y_1(b\gamma)\right] \\ &- \frac{i\pi J_1(b\gamma)}{4\gamma}\left[bk_{\mathrm{r}}\gamma Y_0(a\gamma) - b\left(k_{\mathrm{d}} - \gamma^2\right)Y_1(a\gamma)\right] \end{aligned}$$

$$- \frac{i\pi J_0(a\gamma)}{4\gamma}\left[\left(-ak_{\rm d} + a\gamma^2 + k_{\rm r}\right) Y_0(b\gamma) - bk_{\rm r}\gamma Y_1(b\gamma)\right]$$
$$- \frac{i\pi J_0(b\gamma)}{4\gamma^2}\left[-\gamma\left(-ak_{\rm d} + a\gamma^2 + k_{\rm r}\right) Y_0(a\gamma) - \left(\gamma^2(-ak_{\rm r}+1) + k_{\rm d}\right) Y_1(a\gamma)\right]. \quad \text{(A.51)}$$

Finally the solution as a function of time becomes

$$f(r,t) = k_{\rm r}\int_0^s du G^{(2)}(r, s-u|r_0, 0)\sum_{n=1}^{\infty} h_n^{(2)}(r) e^{-\gamma_n^2 Dt}, \quad \text{(A.52)}$$

where

$$h_n^{(2)}(r) = i\pi\gamma_n \frac{-Y_0(b\gamma_n)J_0(r\gamma_n) + J_0(b\gamma_n)Y_0(r\gamma_n)}{2C_2'(i\gamma_n)}. \quad \text{(A.53)}$$

The full solution becomes

$$\rho^{(2)}(r,t) = G^{(2)}(r,t|r_0,0) + k_{\rm r}\sum_{m,n} h_m^{(2)}(r) g_n^{(2)}(r|r_0)\frac{e^{-\gamma_m^2 Dt} - e^{-\beta_n^2 Dt}}{\beta_n^2 - \gamma_m^2}, \quad \text{(A.54)}$$

where we use the superscript (2) to indicate that this solution pertains to the domain with absorbing outer boundary, to be consistent with the main text. The distribution of $r$, averaged over a time window $[(\ell-1)\Delta t, \ell\Delta t]$, where $\ell = 1, 2, 3, ...$, is then given by

$$\begin{aligned}
\rho_\ell^{(2)}(r) &= \frac{1}{\Delta t}\int_{(\ell-1)\Delta t}^{\ell\Delta t} dt \rho^{(2)}(r,t) \\
&= \sum_n g_n^{(2)}(r|r_0)\frac{e^{-\beta_n^2(\ell-1)D\Delta t}\left[1 - e^{-\beta_n^2 D\Delta t}\right]}{\beta_n^2 D\Delta t} \\
&+ k_{\rm r}\sum_{m,n}\frac{h_m^{(2)}(r)g_n^{(2)}(r|r_0)}{\left(\beta_n^2 - \gamma_m^2\right)D\Delta t}\Big\{\gamma_n^{-2}e^{-\gamma_n^2(\ell-1)D\Delta t}\left[1 - e^{-\gamma_n^2 D\Delta t}\right] \\
&- \beta_n^{-2}e^{-\beta_n^2(\ell-1)D\Delta t}\left[1 - e^{-\beta_n^2 D\Delta t}\right]\Big\} \quad \text{(A.55)}
\end{aligned}$$

## References


[1] von Smoluchowski M 1917 *Z. Physik. Chem.* **92** 129
[2] Collins F C and Kimball G E 1949 *J. Colloid Sci.* **4** 425–437
[3] Naqvi K R, Mork K J and Waldenstrom S 1980 *J. Phys. Chem.* **84** 1315–1319
[4] Agmon N and Szabo A 1990 *J. Chem. Phys.* **92** 5270
[5] Noyes R M 1954 *J. Chem. Phys.* **22** 1349
[6] Van Beijeren H, Dong W and Bocquet L 2001 *J. Chem. Phys.* **114** 6265
[7] Torney D C and McConnell H M 1983 *P. Roy. Soc. Lond.* A Mat. **387** 147–170
[8] Fange D, Berg O G, Sjoberg P and Elf J 2010 *Proc. Natl. Acad. Sci. USA* **107** 19820–19825
[9] Agmon N 1984 *J. Chem. Phys.* **81** 2811
[10] Kim H and Shin K J 1999 *Phys. Rev. Lett.* **82** 1578–1581
[11] Melo E and Martins J 2006 *Biophys. Chem.* **123** 77–94
[12] van Zon J S and ten Wolde P R 2005 *Phys. Rev. Lett.* **94** 128103
[13] Opplestrup T, Bulatov V V, Gilmer G H, Kalos M H and Sadigh B 2006 *Phys. Rev. Lett.* **97** 230602
[14] Carslaw H S and Jaeger J C 1986 *Conduction of Heat in Solids* 2nd ed (Oxford: Clarendon Press)

[15] Koyama-Honda I, Ritchie K, Fujiwara T, Iino R, Murakoshi H, Kasai R S and Kusumi A 2005 *Biophys. J.* **88** 2126–2136
[16] Ruprecht V, Brameshuber M and Schutz G J 2009 *Soft Matter* **6** 568–581
[17] Abramowitz M and Stegun I A 1964 *Handbook of mathematical functions with formulas, graphs, and mathematical tables* (Courier Dover Publications)
[18] Suzuki K G, Fujiwara T K, Edidin M and Kusumi A 2007 *J. Cell. Biol.* **177** 731–742
[19] Kusumi A, Nakada C, Ritchie K, Murase K, Suzuki K, Murakoshi H, Kasai R S, Kondo J and Fujiwara T 2005 *Annu. Rev. Biophys. Biomol. Struct.* **34** 351–378
[20] Nabi I R 2011 *Cellular Membrane Domains* (Hoboken, N.J: Wiley-Blackwell)
[21] Kasai R S, Suzuki K G N, Prossnitz E R, Koyama-Honda I, Nakada C, Fujiwara T K and Kusumi A 2011 *J. Cell. Biol.* **192** 463–480
[22] Destainville N and Salome L 2006 *Biophys. J.* **90** L17–L19
[23] Geyer T and Winter U 2009 *J. Chem. Phys.* **130** 114905
[24] Winter U and Geyer T 2009 *J. Chem. Phys.* **131** 104102
[25] Plimpton S and Slepoy A 2005 *J. Phys. Conf. Ser.* **16** 305–309
[26] Andrews S S and Bray D 2004 *Phys. Biol.* **1** 137–151
[27] Le Novére N and Shimizu T S 2001 *Bioinformatics* **17** 575 –576
[28] Stiles J and Bartol T 2001 Monte Carlo methods for simulating realistic synaptic microphysiology using MCell *Computational neuroscience: Realistic modeling for experimentalists* ed Erik D S (CRC Press, Boca Raton, FL) pp 87–127
[29] Takahashi K, Tanase-Nicola S and ten Wolde P R 2010 *Proc. Natl. Acad. Sci. USA* **107** 2473 –2478
[30] Redner S 2001 *A Guide to First-Passage Processes* (Cambridge, UK: Cambridge University Press)